Thermal cycling and reactivity of a MoSi2/ZrO2 composite designed for self-healing thermal barrier coatings

Franck Nozahic, Daniel Monceau, Claude Estournès

Thermal cycling and reactivity of a MoSi$_2$/ZrO$_2$ composite designed for self-healing thermal barrier coatings

Franck Nozahic [a,b], Daniel Monceau [a,c,*], Claude Estournès [b,c]

[a] CIRIMAT, équipe MEMO, ENSIACET, 4 Allée Emile Monso, 31030 Toulouse, France
[b] Université de Toulouse, UPS, équipe NNC, Institut Carnot Cirimat, 118 Route de Narbonne, F-31062 Toulouse, France
[c] CNRS, Institut Carnot Cirimat, F-31062 Toulouse, France

ABSTRACT

Consolidated (relative density of 84%) composite made of molybdenum di-silicide (MoSi$_2$) particles dispersed in a yttria partially stabilized zirconia matrix (8Y$_2$O$_3$–ZrO$_2$) was prepared by spark plasma sintering. Cyclic oxidation of the composite at temperature ranging from 1000 °C to 1300 °C was studied. Parabolic rate constants (k_p) values of the composite material are in good agreement with those obtained in the literature for the oxidation of bulk MoSi$_2$. Following oxidation exposure, formation of Mo$_5$Si$_3$, SiO$_2$ and ZrSiO$_4$ phases was observed. These observations are compatible with the use of MoSi$_2$ as a self-healing agent in YPSZ thermal barrier coatings.

1. Introduction

Thermal barrier coatings (TBCs) made of yttria partially stabilized zirconia (YPSZ), deposited by plasma-spraying, are widely used to increase the durability of hot-section metal components in advanced gas-turbine for aircrafts and power generation [1–4]. YPSZ is used for high temperature applications due to its mechanical strength and chemical stability at such temperatures. However, as a ceramic, YPSZ suffers from a relatively low toughness. TBCs failure is governed by a sequence of initiation, propagation and coalescence of cracks that leads to spallation of the TBC, exposing the hot-section metal components to the high-temperature environment [5]. Hence, a TBC that is capable of autonomic crack repair and structural integrity recovery in a high-temperature oxidizing environment is highly desirable. Recently, Sloof et al. [6,7] proposed the concept of a new self-healing thermal barrier coating based on the oxidation of boron doped molybdenum di-silicide (B-MoSi$_2$) healing particles embedded in the ZrO$_2$-based TBC. Healing particles intercepted by cracks will oxidize preferentially, leading to the formation of amorphous SiO$_2$, which flows into cracks and establishes direct contact with the crack faces. The wetting of the crack faces is followed by a chemical reaction with the ZrO$_2$-based TBC coating leading to the formation of a load bearing ZrSiO$_4$ phase.

MoSi$_2$ exhibits a high melting point (2020 °C) [8], it has a density close to YPSZ (MoSi$_2$ = 6.24 g·cm^{-3}, YPSZ = 6.08 g·cm^{-3}) [8,9], it shows a high oxidation resistance at elevated temperature, and its coefficient of thermal expansion (CTE) matches reasonably with the one of YPSZ (MoSi$_2$ = 8.1 × 10^{-6} °C^{-1}, stabilized ZrO$_2$ = 10 × 10^{-6} °C^{-1}) [10,11] which means that thermal stresses induced by the mismatch of the respective CTEs will be minimal. YPSZ are widely used as solid electrolytes in Solid Oxides Fuel Cells (SOFC) since they are recognized as oxygen ion conductors at elevated temperatures [12,13]. Meaning that oxygen ion can pass easily through the YPSZ matrix to oxidize the dispersed MoSi$_2$ particles.

For the current work, a partially densified composite (relative density of 84%) made of a YPSZ matrix containing 20 wt.% of MoSi$_2$ particles has been prepared using spark plasma sintering (SPS). The high temperature behavior of such composite under air atmosphere has been studied using Cyclic Thermogravimetric Analysis (CTGA) [14] and the phase transformations during the process have been examined.

2. Experimental procedure

Appropriate amounts of YPSZ containing 7–8 wt.% Y$_2$O$_3$ (average grain size: 45 μm) and MoSi$_2$ (average grain size: 19 μm) particles were mechanically dry mixed for 1 h in a Turbula-type powder blender. The volume fraction of MoSi$_2$ particles was 20%. The composite material (referred as YSZ-20MoSi$_2$) used in this study was produced with a Dr. Sinter SPS-2080 equipment (SPS Syntex Inc., Kanagawa, JP) located at the Plateforme Nationale de Frittage Flash (PNF2, CNRS CIRIMAT,

Université Toulouse III Paul Sabatier, France). A 30 mm inner diameter graphite die covered with a graphite foil (Papyex® Mersen) was filled with the powder mixture and mounted into the SPS equipment. SPS was completed with a fixed heating rate of 100 °C·min^{-1}, up to 1500 °C, with a soaking time of 5 min at this temperature and under a constant macroscopic compaction uni-axial pressure of 100 MPa applied since the beginning of the sintering cycle. The temperature was monitored by an optical pyrometer focused on a small hole (3 mm in depth) located at the external surface of the die. The electric current was applied by pulses following the standard 12/2 (on/off 3.3 ms) pulse pattern. The relative density of the sample was about 84% after SPS. Such level of porosity (16 vol.%) was performed in order to reproduce the one of industrial TBC. A specimen of $10 \times 10 \times 2$ mm^3 with parallelepiped-like shape was cut from the sintered sample. All surfaces were wet grinded using SiC papers down to P600.

Cyclic oxidation experiment was performed on this specimen in flowing synthetic dry air (flux = 5 ml·min^{-1}, gas velocity = 0.85 mm·s^{-1}), using a commercial thermobalance (Setaram TAG24s). The experiment consisted of 10 cycles at 1000 °C followed by 10 cycles at 1100 °C, 1200 °C and 1300 °C, with dwell times of 3600 s at high temperature and 6250 s down to 50 °C. Heating rate and initial cooling rate were controlled at 60 °C·min^{-1} and data were recorded in real time, including during heating and cooling.

Following the above mentioned oxidation test, the specimen was promptly removed from the equipment and polished with 1 μm diamond suspension. The cross-section was examined by a scanning electron microscope (LEO435VP) equipped with an energy dispersive X-ray (EDX) spectroscopy system. The oxidized specimen was investigated by X-ray diffraction (XRD) for phase identification. Image analysis was performed using the "Image J" software to determine the surface percentages of the different phases of the material after oxidation.

3. Results and discussion

3.1. Synthesis of the YSZ–20MoSi$_2$ composite

The microstructure and the XRD pattern of the sintered composite (referred as YSZ–20MoSi$_2$) are shown in Fig. 1 and Fig. 2(a). Results of the XRD analysis of the composite after cyclic oxidation (Fig. 2(b)) will be discussed later. It can be observed that the MoSi$_2$ particles are homogeneously distributed in the YPSZ matrix. Based on the analysis of optical microscope images, the level of porosity is estimated to be 16 vol.%. XRD of the composite indicates that it consists of tetragonal zirconia and tetragonal MoSi$_2$ and that no visible reaction has occurred between the YPSZ matrix and the MoSi$_2$ particles as a result of the sintering process.
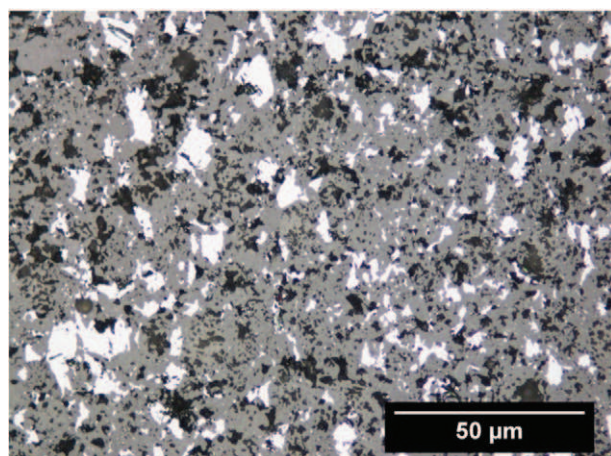

Fig. 1. Cross-section of the composite observed with optical microscope showing MoSi$_2$ particles (white), YPSZ matrix (light gray) and porosities (dark gray).
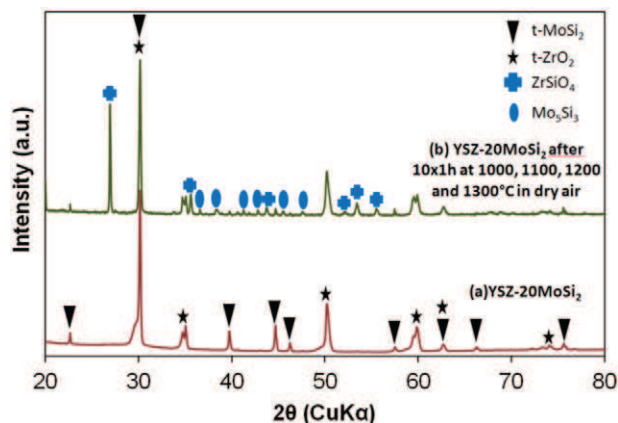

Fig. 2. XRD patterns of: (a) sintered YSZ–20MoSi$_2$ composite; (b) sintered YSZ–20MoSi$_2$ composite exposed to flowing dry air for 10×1 h at 1000, 1100, 1200 and 1300 °C.

3.2. Cyclic oxidation of the YSZ–20MoSi$_2$ composite in air

The plot of the net mass change versus time for cyclic oxidation of the composite at 1000, 1100, 1200, 1300 °C is shown in Fig. 3. A parabola-like shape is observed for all temperature regimes. A SEM micrograph of a cross section of the oxidized material after the complete cyclic oxidation experiment is given in Fig. 4(a). No visible cracks were observed resulting from stresses that would be induced either by volume increase caused by oxide growth or thermally induced by different CTE of grown oxides, MoSi$_2$ particles and YPSZ matrix. This is consistent with a previous work of Petrovic and Honnell [15] on MoSi$_2$ composites containing PSZ inclusions prepared by hot pressing. A continuous layer of silica with a uniform thickness of 0.6 μm is observed around MoSi$_2$ particles as a result of the selective oxidation of silicon from the MoSi$_2$ substrate, according to the Eq. (1) [16].

$$5MoSi_{2(s)} + 7O_{2(g)} \rightarrow Mo_5Si_{3(s)} + 7SiO_{2(s)} \qquad (1)$$

The formation of a dense protective SiO$_2$ scale, above 1000 °C, is responsible for the high oxidation resistance of MoSi$_2$ [17]. The low oxygen partial pressure at the SiO$_2$/MoSi$_2$ interface prevents the formation of volatile MoO$_3$. XRD analysis (Fig. 2(b)) did not enable to identify the structural type of the silica layer. According to Berztiss et al. [8], silica formed on MoSi$_2$ was found to be in the amorphous state up to 1700 °C, while two other research groups claimed that the silica scale has a crystalline structure of tridymite from 1000 to 1200 °C [16] and cristobalite from 1300 to 1400 °C [16,18].

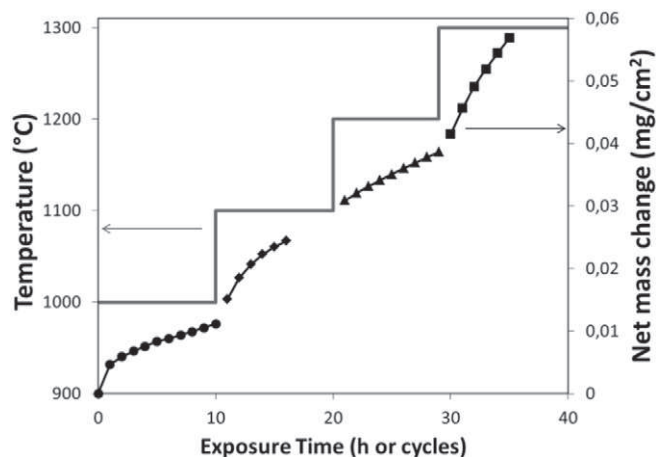**Fig. 3.** Evolution of the net mass change of the composite sample exposed to flowing dry air for 10×1 h at 1000, 1100, 1200 and 1300 °C in a cyclic thermogravimetric apparatus.
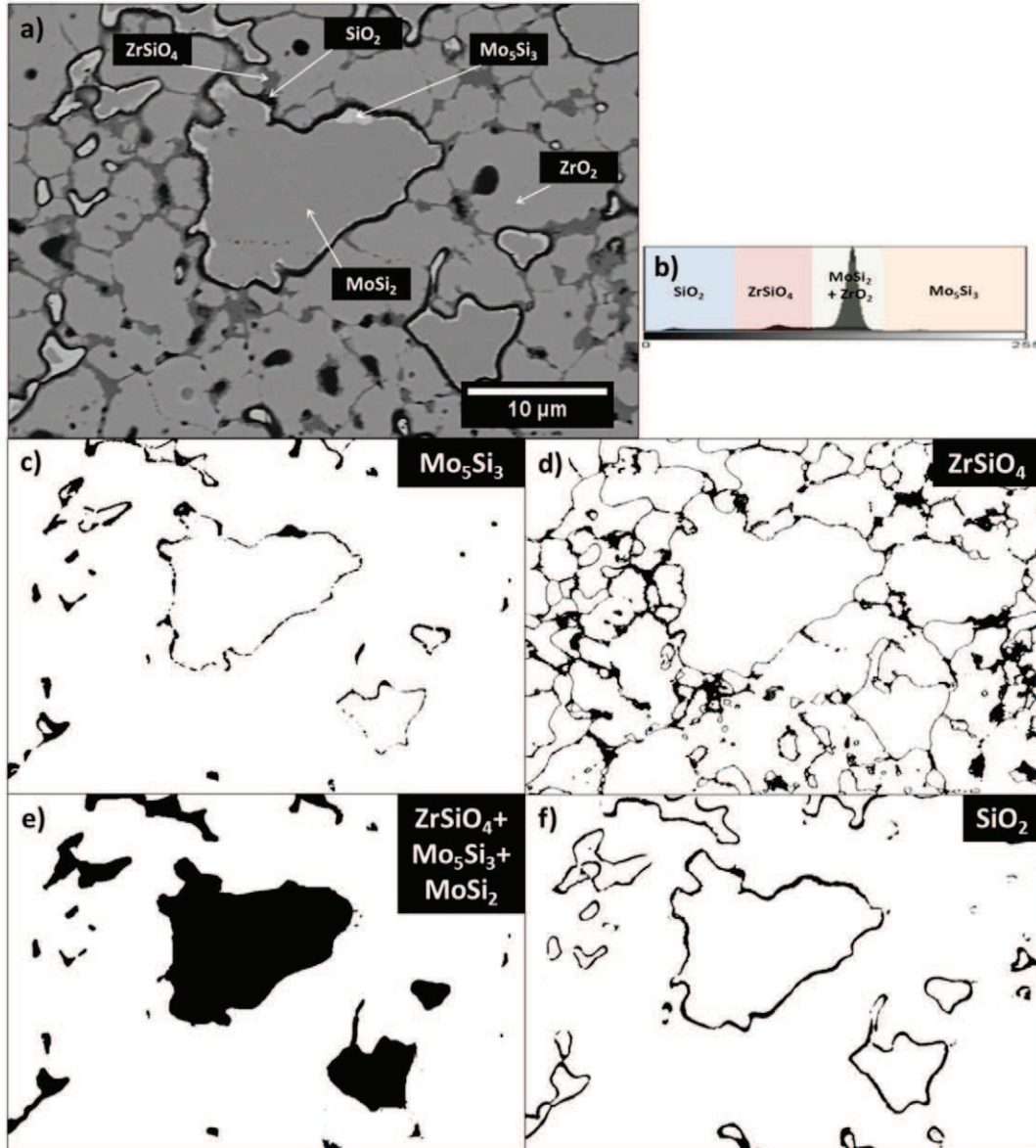
Fig. 4. Cross section BSE image of the composite sample exposed to flowing dry air for 10 × 1 h at 1000, 1100, 1200 and 1300 °C (a) and example of image analysis on the composite: (b) gray value histogram of the BSE image (0 = pure black, 255 = pure white); (c, d, e, f) thresholding of the different phases.

A Mo_5Si_3 phase, in lighter gray than the other two phases, is observed at the surface of the $MoSi_2$ particles in contact with a SiO_2 layer, highlighting a local silicon depletion in this zone. The formation of this phase leads to rapid consumption of Si through oxidation to form the silica layer and is in agreement with the thermodynamic predictions (Eq. (1)). Further dissociation of Mo_5Si_3 is not necessary to achieve the growth of the silica scale because the diffusion rate of silicon in Mo_5Si_3 is considerably higher than the diffusion rate of the oxygen in SiO_2 for temperatures above 1200 °C [19]. However, in case of contact with high oxygen partial pressure (PO_2), Mo_5Si_3 can be further oxidized into MoO_3 and SiO_2 following Eq. (2) [16].

$$2Mo_5Si_{3(s)} + 21O_{2(g)} \rightarrow 10MoO_{3(g)} + 6SiO_{2(s)} \tag{2}$$

Complete silicon and molybdenum exhaustion can be observed for small particles leading to the disappearance of the Mo_5Si_3 phase for longer oxidation times, as reported by Zhu et al. [16]. In this case, Mo_5Si_3 is fully oxidized into MoO_3 and SiO_2 according to Eq. (2).

An additional phase $ZrSiO_4$ is observed as a result of the reaction between the SiO_2 phase and the ZrO_2 matrix according to Eq. (3) [20].

$$SiO_{2(s)} + ZrO_{2(s)} \rightarrow ZrSiO_{4(s)} \tag{3}$$

According to the ZrO_2–SiO_2 phase diagram, proposed by Butterman and Foster [21], pure zircon is a stable phase that decomposes into t-ZrO_2 and SiO_2 (cristobalite) at a temperature approximately 1676 °C. The formation of zircon at a temperature as low as 1300 °C is in agreement with previous studies [20,22]. According to Itoh [20], zircon starts forming around 1200 °C and results exclusively from the reaction between amorphous silica and tetragonal zirconia. This reaction is supposed to predominate the transformation of amorphous silica into cristobalite. Mao and Sloof [22] affirmed that zircon can form at 1100 °C in air from cold pressed mixtures of YPSZ and $MoSi_2$ powders.

In the present study, it was observed that a layer of zircon, with a thickness of about 0.5 µm, is formed around the original $MoSi_2$ particles, between the silica scale and the zirconia matrix. It should be noted that zircon is also located at the zirconia grain boundaries at a distance up to 19 µm away from the $MoSi_2$ particle. The thickness of the zircon located
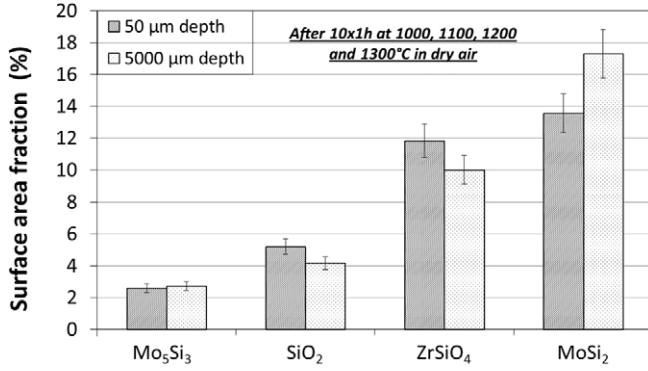
Fig. 5. Surface area fractions of the different phases after oxidation of 10×1 h at 1000, 1100, 1200 and 1300 °C in flowing dry air.

at the grain boundaries is 2.5 times as high as the thickness of the zircon located at the interface between $MoSi_2$ particles and the surrounding YPSZ grains. This implies that atomic diffusion of silicon in solid state can proceed, in the grains boundaries of the YPSZ matrix, at long distances from the $MoSi_2$ particles. This observation is of interest for the concept of a self-healing TBC [6]. According to Veytizou et al. [23] and marker experiments of Eppler [24], it is suggested that Si^{4+} is the fastest cation. Leading to the deduction that its diffusion through the zircon layer is the limiting step of the zircon formation mechanism at the zircon/zirconia interface.

Image analysis was performed to determine surface percentages of the different phases of the material after oxidation (Fig. 4). Plots of the surface area fractions of the different phases of the composite after oxidation and for different depths from the surface are shown in Fig. 5. The fraction of zirconia transformed into zircon is about 16% after the overall cyclic oxidation experiment. The phase fractions of SiO_2 and $ZrSiO_4$ at 50 μm depth are 24% and 18% higher than those at 5000 μm depth respectively. However, the diffusion rate of oxygen in Y_2O_3-doped ZrO_2 is several orders of magnitude higher than the diffusion rates of the oxygen in SiO_2 and $ZrSiO_4$ for temperatures above 1000 °C [25–28]. This means that zircon formed at the grain boundaries of the YPSZ matrix acts as a diffusion barrier for oxygen in-depth ingress in the material, just by decreasing the diffusion section (i.e. the ZrO_2 volume fraction). The increase of the amount of oxygen in the specimen was estimated by measuring the fraction of SiO_2 and $ZrSiO_4$. The estimated mass gain due to oxygen uptake in $ZrSiO_4$ and SiO_2 grow is in close match with the one measured from the CTGA experiment (46 and 42 mg respectively). This indicates that if MoO_3 sublimation occurs, it is limited. Furthermore, no MoO_3 crystals were found in the silica scale after cooling from the oxidation tests or deposited in the cooler parts of the apparatus. No signs of bubbling were observed. This confirms that, in these conditions, the formation of a dense silica scale prevents or drastically reduces MoO_3 evaporation in this case.

3.3. Discussion

Plotting the oxidation-induced net mass change versus time shows a large mass gain for a silica former material (Fig. 3). This is explained by the large surface area of the reacting $MoSi_2$ particles. The total surface of the oxidation-reactive surface for the $MoSi_2$ particles embedded in the zirconia matrix was determined prior to oxidation tests by using

image analysis technique. A surface area of 683 cm^2 was measured, which is almost 200 times higher than the geometrical external surface area of the specimen. As a first approximation, parabolic rate constants (k_p) were determined by considering a constant reactive surface even though the surface is expected to slightly decrease with time. The fitting of the thermogravimetric curves by a complete parabolic law enabled to determine k_p values at different temperatures, independently of the net mass change due to oxidation at lower temperatures [29]. These k_p values are given in Table 1. No mass loss was observed due to a transient oxidation mechanism with competitive oxidation of silicon and molybdenum leading to the formation of a non-protective silica layer and volatile MoO_3, as observed by Knittel et al. [30]. A continuous mass gain was observed for all oxidation temperatures.

At the starting oxidation temperature of 1000 °C, high initial mass gain is observed prior to the establishment of a protective silica layer forming a diffusion barrier. For these temperature regimes, the oxidation of $MoSi_2$ covered by a dense and protective layer is known to be controlled by the slow inward diffusion of oxygen through the silica layer [31]. A clear weight gain is observed when changing temperature regime and then slowed down for longer oxidation times. The k_p value of the composite material at 1300 °C is 12 times higher than at 1000 °C. Despite the approximation concerning the constant surface area of the particles, the k_p values of the composite material are in good agreement with those obtained in the literature for the oxidation of bulk $MoSi_2$ [18, 30].

The thickness of the silica layer can be compared with the one calculated from the mass gain assuming that mass gain is predominantly due to oxygen uptake to grow silica. The predicted thickness is 1 μm by using a k_p value of 3.97×10^{-7} $mg^2 \cdot cm^{-4} \cdot s^{-1}$ for a uniaxial hot pressed $MoSi_2$ in air at 1300 °C for 10 h obtained by Knittel et al. [30]. Thus, the measured thickness of the silica layer is 40% thinner than expected when considering only oxygen uptake to form silica. This can be explained by the fact that the measured mass change is the sum of the contribution of high oxygen mass gain caused by formation of both $ZrSiO_4$ and SiO_2 and small mass loss due to possible evaporation of MoO_3. The growth of $ZrSiO_4$ from ZrO_2 and SiO_2 decreases the thickness of the protective layer of SiO_2. Therefore this layer is a less effective diffusion barrier for oxygen ingress and the oxidation kinetics are expected to slightly increase. But the $ZrSiO_4$ layer on top of the silica is also a diffusion barrier which could decrease the oxidation kinetics of silicon. More generally, a general kinetic model which takes into account the diffusion of the species in the multiple layers of the system, and perhaps also the rates of reaction at the interfaces, needs to be built to fully assess the oxidation-kinetics of the ZrO_2–$MoSi_2$ composite.

4. Conclusion

Consolidated (relative density of 84%) composite made of $MoSi_2$ particles dispersed in a yttria partially stabilized ZrO_2 matrix has been prepared by SPS. The oxidation of the composite under dry air for 10 h at 1000/1100/1200/1300 °C has been investigated. The oxidation parabolic rate constant k_p values of the composite material are in fair agreement with those reported in the literature for the oxidation of bulk $MoSi_2$, taking into account that the reactive surface area is the one of the embedded $MoSi_2$ particles and despite the geometric and kinetics approximations that were used. The oxidation results in the formation of a continuous SiO_2 layer around $MoSi_2$ particles. Mo_5Si_3 phase is formed under the silica scale due to a local silicon depletion zone

Table 1

Parabolic rate constants values (k_p) of the Y_2O_3-partially stabilized ZrO_2 dispersed $MoSi_2$ particles composite and k_p values from the literature for bulk $MoSi_2$ materials.

Temperature (°C)		1000	1100	1200	1300
k_p ($mg^2 \cdot cm^{-4} \cdot s^{-1}$)	Present study	3.0×10^{-9}	6.3×10^{-9}	1.2×10^{-8}	3.7×10^{-8}
	Knittel et al. [30]	2.1×10^{-9}	x	4.7×10^{-8}	4.0×10^{-7}
	Meilsheimer et al. [18]	2.1×10^{-8}	4.7×10^{-8}	x	x

formed at the surface of the MoSi₂ particles. For long exposition times, an additional ZrSiO₄ phase is observed as a result of the reaction between formed silica and YPSZ matrix. ZrSiO₄ is formed both around the MoSi₂ particles and at the grain boundaries of the YPSZ matrix. The ZrSiO₄ layer formed around the silica layer does not affect much the oxidation kinetics. Also, it is interesting to note that ZrSiO₄ is observed far away from the MoSi₂ particles. This can be very beneficial for the self-healing mechanism of the composite.

Acknowledgments

References

[1] R.A. Miller, Thermal barrier coatings for aircraft engines: history and directions, J. Therm. Spray Technol. 6 (1997) 35–42.
[2] S. Bose, J. DeMasi-Marcin, Thermal barrier coating experience in gas turbine engines at Pratt & Whitney, J. Therm. Spray Technol. 6 (1997) 99–104.
[3] M.J. Stiger, N.M. Yanar, M.G. Topping, F.S. Pettit, G.H. Meier, Thermal barrier coatings for the 21st century, Z. Met. 90 (1999) 1069–1078.
[4] N.P. Padture, M. Gell, E.H. Jordan, Thermal barrier coatings for gas-turbine engine applications, Science's Compass 280-4 (2002).
[5] A.G. Evans, D.R. Mumm, J.W. Hutchinson, G.H. Meier, F.S. Pettit, Mechanisms controlling the durability of thermal barrier coatings, Prog. Mater. Sci. 46 (2001) 505–553.
[6] W.G. Sloof, S.R. Turteltaub, A.L. Carabat, Z. Derelioglu, S.A. Ponnusami, G.M. Song, Crack healing in yttria stabilized zirconia thermal barrier coatings, Self healing Materials — Pioneering Research in Netherlands 2015, pp. 217–225.
[7] Z. Derelioglu, A.L. Carabat, G.M. Song, S. van der Zwaag, W.G. Sloof, On the use of B-alloyed MoSi₂ particles as crack healing agents in yttria stabilized zirconia thermal barrier coatings, J. Eur. Ceram. Soc. 35 (16) (2015) 4507–4511.
[8] D.A. Berztiss, R.R. Cerchiara, E.A. Gulbransen, F.S. Pettit, G.H. Meier, Proceedings of the First High Temperature Structural Silicides Workshop Oxidation of MoSi₂ and comparison with other silicide materials, Mater. Sci. Eng. A 155 (1992) 165–181.
[9] E. Withey, C. Petorak, R. Trice, G. Dickinson, T. Taylor, Design of 7 wt.% Y₂O₃–ZrO₂/mullite plasma-sprayed composite coatings for increased creep resistance, J. Eur. Ceram. Soc. 27 (2007) 4675–4683.
[10] A.K. Vasudévan, J.J. Petrovic, A comparative overview of molybdenum disilicide composites, Mater. Sci. Eng. A 155 (1992) 1–17.
[11] E. Medvedovski, Wear-resistant engineering ceramics, Wear 249 (2001) 821–828.
[12] S.J. Skinner, J.A. Kilner, Oxygen ion conductors, Materials Today 6 (2003) 30–37.
[13] A.J. McEvoy, Thin SOFC electrolytes and their interfaces: a near-term research strategy, Solid State Ionics 132 (2000) 159–165.
[14] A. Vande Put, D. Monceau, D. Oquab, Cyclic thermogravimetry of TBC system, Surf. Coat. Technol. 202 (2007) 665–669.
[15] J.J. Petrovic, R.E. Honnell, Partially stabilized ZrO₂ particle–MoSi₂ matrix composites, J. Mater. Sci. 25 (1990) 4453–4456.
[16] Y.T. Zhu, M. Stan, S.D. Conzone, D.P. Butt, Thermal oxidation kinetics of MoSi₂-based powders, J. Am. Ceram. Soc. 82 (1999) 2785–2790.
[17] S. Lohfeld, M. Schütze, A. Böhm, V. Güther, R. Rix, R. Scholl, Oxidation behaviour of particle reinforced MoSi₂ composites at temperatures up to 1700 °C, Mater. Corros. 56 (2005) 250–258.
[18] S. Melsheimer, M. Fietzek, V. Kolarik, A. Rahmel, M. Schutze, Oxidation of the intermetallics MoSi₂ and TiSi₂: a comparison, Oxid. Met. 47 (1997) 139–203.
[19] R.W. Bartlett, P.R. Gage, Diffusion kinetics affecting formation of silicide coatings on molybdenum and tungsten, Trans. AIME 233 (1965) 968.
[20] T. Itoh, Formation of polycristalline zircon (ZrSiO₄) from amorphous silica and amorphous zirconia, Crystal Growth 125 (1992) 223–228.
[21] W.C. Butterman, W.R. Foster, Zircon stability and the ZrO₂–SiO₂ phase diagram, Am. Mineral. 52 (1967) 880–885.
[22] W. Mao, W. Sloof, Kinetics of Self-healing Reaction in TBC with MoSi₂ Based Sacrificial Particles, 2013.
[23] C. Veytizou, J.F. Quinson, O. Valfort, G. Thomas, Zircon formation from amorphous silica and tetragonal zirconia: kinetic study and modelling, Solid State Ionics 139 (2001) 315–323.
[24] R.A. Eppler, Mechanism of formation of zircon stains, J. Am. Ceram. Soc. 53 (1970).
[25] M.A. Lamkin, F.L. Riley, R.J. Fordham, Oxygen mobility in silicon dioxide and silicate glasses: a review, J. Eur. Ceram. Soc. 10 (1992) 347–367.
[26] M.S. Khan, M.S. Islam, D.R. Bates, Cation doping and oxygen diffusion in zirconia: a combined atomistic simulation and molecular dynamics study, J. Mater. Chem. 8 (1998) 2299–2307.
[27] X. Li, B. Hafskjold, Molecular dynamics simulations of yttrium-stabilized zirconia, J. Phys. Condens. Matter 7 (1995) 1255.
[28] B. Zhang, X. Wu, Prediction of self-diffusion and heterodiffusion coefficients in zircon, J. Asian Earth Sci. 42 (2011) 134–141.
[29] D. Monceau, B. Pieraggi, Determination of parabolic rate Constants from a local analysis of mass gain curves, Oxid. Met. 50 (5) (1998) 477–493.
[30] S. Knittel, S. Mathieu, M. Vilasi, The oxidation behaviour of uniaxial hot pressed MoSi₂ in air from 400 to 1400 °C, Intermetallics 19 (2011) 1207–1215.
[31] C.D. Wirkus, D.R. Wilder, High temperature oxidation of molybdenum disilicide, J. Am. Ceram. Soc. 49 (1966) 173–177.